Available online at www.sciencedirect.com
SCIENCE DIRECT
Journal of the European Ceramic Society 26 (2006) 1267–1272
www.elsevier.com/locate/jeurceramsoc

Grain boundary crystallization during furnace cooling of α-SiC sintered with Y_2O_3–Al_2O_3–CaO

Je-Hun Lee [a], Doh-Yeon Kim [a], Young-Wook Kim [b,*]

[a] *Center for Microstructure Science of Materials and School of Material Science and Engineering, College of Engineering, Seoul National University, Seoul 151-744, South Korea*
[b] *The University of Seoul, Department of Materials Science and Engineering, 90 Jeonnong-Dong, Dongdaemoon-Ku, Seoul 130-743, South Korea*

Received 5 September 2004; received in revised form 27 December 2004; accepted 10 January 2005
Available online 23 February 2005

Abstract

For the SiC specimens prepared with Al_2O_3, Y_2O_3, and CaO (AYC-SiC), it was observed that the intergranular films and triple-junction phases were completely crystallized without subsequent heat-treatment after sintering. The intergranular films were determined to have hetero-epitaxially grown $(Al,Si)_2OC$ of a 2H-type wurtzite structure, with partial substitution of Al by Si. Segregation of Ca and Y at the grain boundaries was also detected by energy-dispersive X-ray spectroscopy (EDS). On the other hand, the composition and structure of the triple junction phases were different from those of intergranular films. It showed hexagonal structure and topotactic relationships with SiC grains ($\boldsymbol{a}_{SiC}//\boldsymbol{a}_{junction}$, $\boldsymbol{c}_{SiC}//\boldsymbol{c}_{junction}$, and $\boldsymbol{a}_{SiC} = 2\boldsymbol{a}_{junction}$).

Keywords: Grain boundary; Liquid phase sintering; SiC; Crystallization

1. Introduction

Densification of silicon carbide (SiC) is usually achieved by the liquid forming additives such as Al_2O_3–Y_2O_3[1–5] or Al–B–C,[6] and it has been reported that the properties of liquid-phase sintered SiC depend critically on the size and shape of the SiC grains as well as the amount and chemistry of the grain boundary phase.[6–9] Materials with an equiaxed and fine-grained microstructure show a high room-temperature strength, while materials with a platelet and coarse-grained microstructure exhibit a high fracture toughness.[5]

Although the densification of SiC is greatly enhanced by the liquid forming additives, they are also responsible for the degradation of mechanical properties at high-temperature. Note that the glassy phase remaining at the grain boundaries of SiC becomes soft at above a certain temperature. Therefore, several strategies have been sought to amend the high-temperature mechanical properties of SiC: (1) the crystallization of the amorphous grain boundary phase by a post-sintering heat-treatment;[10–13] (2) the formation of a transient liquid-phase;[14] (3) the reduction of the overall additive content by colloidal processing;[15] and (4) the use of refractive additives, such as AlN and Y_2O_3.[16] Among them, the crystallization of the grain boundary phase by post-sintering heat-treatment at 1100–1300 °C is known[10–13,17,18] to be quite effective for increasing the high temperature strength and creep resistance of SiC. However, the inconvenience is that the process requires an extensive heat-treatment up to 500 h.[10–13] It is, therefore, worth searching the sintering additives, which lead to the crystallization of grain boundary phase without prolonged heat-treatment.

For this purpose, we used Al_2O_3, Y_2O_3 and CaO, for the densification of α-SiC (AYC-SiC). Note that the eutectic liquids[19] of the system Al_2O_3–Y_2O_3–CaO appear at lower temperature (~1400 °C in 32 mol% Al_2O_3, 7 mol% Y_2O_3 and 61 mol% CaO) than those obtained with traditional Al_2O_3 and Y_2O_3 (AY-SiC). In this regard, the viscosity of a liquid appeared during sintering of AYC-SiC is expected to

* Corresponding author. Tel.: +82 2 2210 2760; fax: +82 2 2215 5863.
E-mail address: ywkim@uos.ac.kr (Y.-W. Kim).

0955-2219/$ – see front matter © 2005 Elsevier Ltd. All rights reserved.
doi:10.1016/j.jeurceramsoc.2005.01.050

be lower compared to that in AY-SiC. Since the low viscosity liquids exhibit small activation energy for diffusion,[20,21] the crystallization process during cooling would to be faster in AYC-SiC. With AYC-SiC specimens, therefore, we examined the possible crystallization of the grain boundary phase without subsequent heat-treatment after sintering.

2. Experimental procedure

Commercially available two kinds of α-SiC powders were used (A-1 grade, Showa Denko, Tokyo, Japan and FCP-15c, Norton AS, Lillesand, Norway) with Al_2O_3 (99.9% pure, Sumitomo Chemical Co., Tokyo, Japan), Y_2O_3 (99.9% pure, Shin-Etsu Chemical Co., Tokyo, Japan), and CaO (99.9% pure, Kojundo Chemical Laboratory Co., Sakado, Japan) powders. The mean particle sizes of the A-1 and FCP-15c α-SiC powders were 0.45 and 0.50 μm, respectively. A mixture of 90 wt.% α-SiC, consisting of 80 wt.% A-1 and 10 wt.% FCP-15c, with 5.7 wt.% Al_2O_3, 3.3 wt.% Y_2O_3, and 1 wt.% CaO was milled in ethanol for 24 h using SiC media. The powder mixture was dried, subsequently sieved through a 60-mesh screen. The powder compacts obtained were sintered at 1900 °C for 4 h under a pressure of 25 MPa in an argon atmosphere. The specimens were furnace-cooled and the applied pressure was removed at 1200 °C. The heating rate was 20 °C/min, and the cooling rate was ∼40 °C/min from 1900 to 1200 °C. The relative density of the specimen was determined by the Archimedes method using deionized water as an immersion medium. X-ray diffraction (XRD) using Cu Kα radiation was performed on ground powders of the specimens.

For HREM observation, SiC disks with a 3 mm-diameter and ∼100 μm-thick were prepared by grinding and cutting. They were mechanically thinned by dimpler (VCR group) up to ∼20 μm thickness and perforated by Ar ion milling (PIPS: Gatan). HREM characterization was performed using a 300 kV field emission transmission electron microscope (JEM 3000F) with a resolution of 1.7 nm. The grain boundary chemistry was analyzed using energy-dispersive X-ray spectroscopy (EDS) equipped with atmospheric tin window (ATW) detector. In the present study, 2.5 nm spot size was used for EDS point analysis. The software program of quantitative or qualitative EDS analyses was an INCA system (Oxford Instruments), where an internal standard was used in determining Cliff–Lorimer factors (*k*-factors).

3. Results and discussion

The AYC-SiC specimens obtained by sintering at 1900 °C under pressure were almost fully dense and its relative density was ∼99.0%. Fig. 1 is the microstructure of the specimen obtained. It showed a typical bimodal size distribution of grains with abnormally grown large-elongated α-SiC grains and relatively small-equiaxed α-SiC grains. The elongated

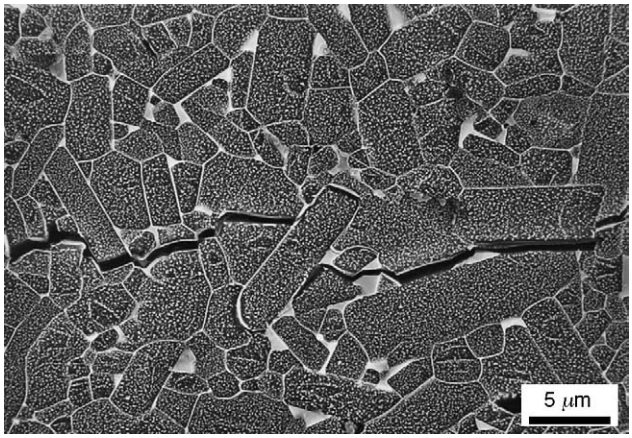

Fig. 1. SEM micrograph of AYC-SiC in as prepared specimen.

large grains were determined to always exhibit well developed basal planes. By the indentation, on the other hand, the cracks were observed to propagate mainly along the grain boundary phase as can be noted from the figure. Phase analysis by XRD showed that the major phase of the specimen was α-6H SiC and the minor phase was α-4H SiC.

Fig. 2 shows a detailed microstructure of the specimen; the upper grain is abnormally grown large one and the interface formed at basal plane was examined. From this, it is noteworthy that no amorphous films were observed at the boundaries even though the specimens were just furnace cooled. Instead, hetero-epitaxially crystallized intergranular films were always detected between SiC grains. The lattice image of crystallized intergranular film shown in Fig. 2 was taken at $[2\,\bar{1}\,\bar{1}\,0]$ zone axis. For SiC specimens prepared with Al, B and C (ABC-SiC), on the other hand, it has been reported that the crystallization of the intergranular phase was only possible by prolonged heat-treatment (1100–1500 °C/85–840 h) after sintering.[10–13]

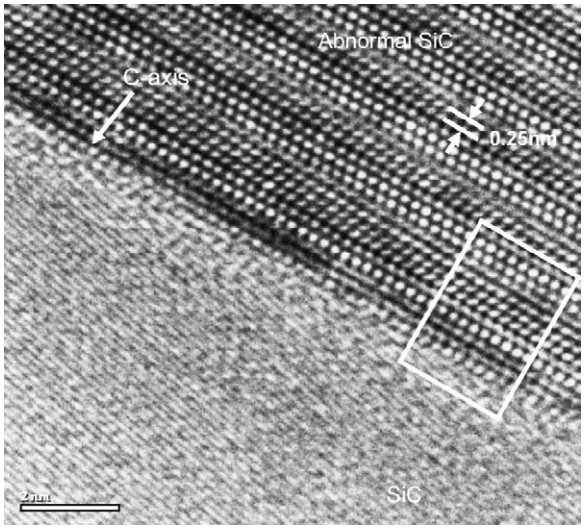

Fig. 2. HRTEM micrograph of the crystallized grain boundary in as prepared AYC-SiC.

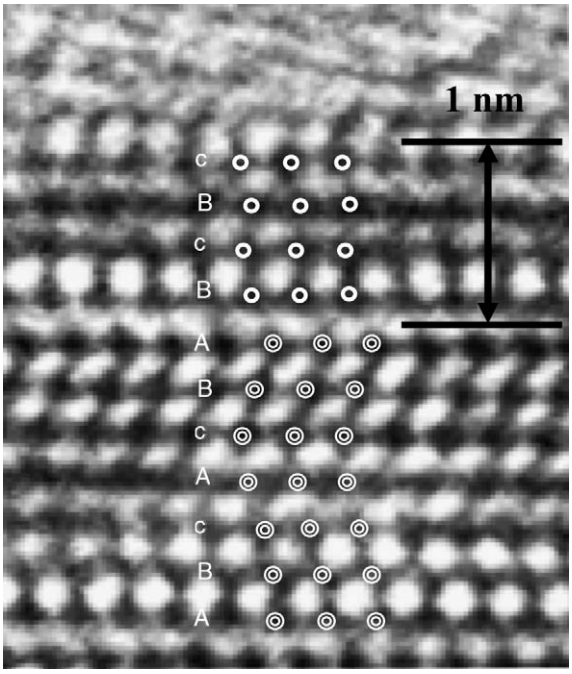

Fig. 3. Magnified HRTEM micrograph of rectangulary enclosed area in Fig. 2.

Fig. 3 is a detailed image of the boundary area marked by a rectangle in Fig. 2. From the circles corresponding to the lattice points, the crystallized boundary layer is well discerned. Interesting point is that there is an abrupt change of the atomic arrangement from 6H-type (ABCACBA. . .) to 2H-type (ABA. . .). Nanobeam diffraction (NBD) with a probe size of ∼1 nm on this intergranular films showed only 6H-type diffraction pattern, where (0 0 0 3) spot of 6H-SiC could be overlapped with (0 0 0 1) spot of 2H-type heteroepitaxially crystallized films at [2 1 1 0] zone axis. The film thickness shown in Fig. 3 was 0.75 nm but others varied from 0.5 to 1 nm.

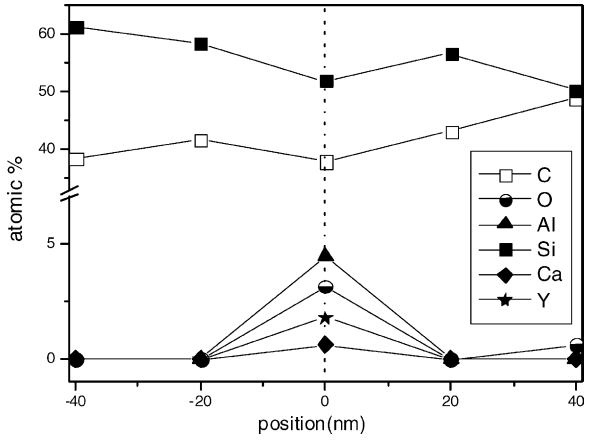

Fig. 4. EDS profile across SiC grain boundaries.

EDS analysis across the grain boundaries was performed with a 2.5 nm-diameter electron probe and the result is shown in Fig. 4. As can be noted, the boundary phase is composed of additives (Al, Y, Ca, and O) elements in which Si and C are dissolved. High concentrations of Si and C are likely to be due to the probe size which is still much larger than film thickness. Since the ionic sizes of Ca^{2+} (0.1000 nm) and Y^{3+} (0.0900 nm) are quite different from that of Al^{3+} (0.0390 nm), substitution of Al by Ca or Y is not expected to occur. In contrast, the ionic size of Si^{4+} (0.0270 nm) is similar to that of Al. Thus, Si is expected to substitute Al in the crystallized films, as identified by Zhang et al.[13] The HREM image (Fig. 3) and the EDS results (Fig. 4) suggest that the crystallized intergranular films are $(Al,Si)_2OC$ with a 2H-type wurtzite structure, where Al is partially substituted by Si. The $(Al,Si)_2OC$ with a 2H-type wurtzite structure in AYC-SiC is the same with the grain boundary structure obtained in ABC-SiC.[13]

Fig. 5(a) is the bright field image of triple-junction phase bounded by large elongated SiC grains and Fig. 5(b) shows EDS results along the dotted line marked in Fig. 5(a). The

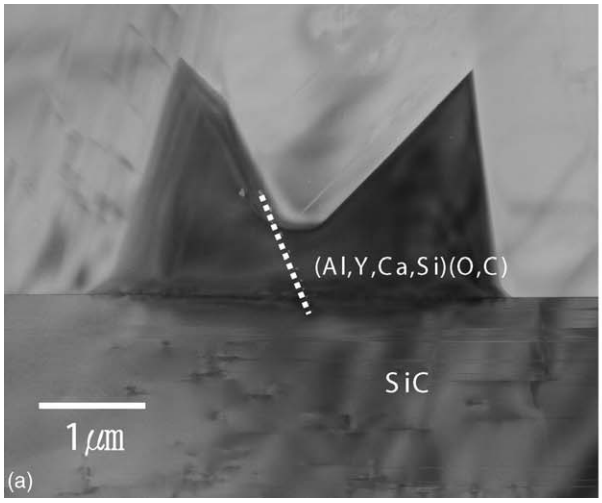

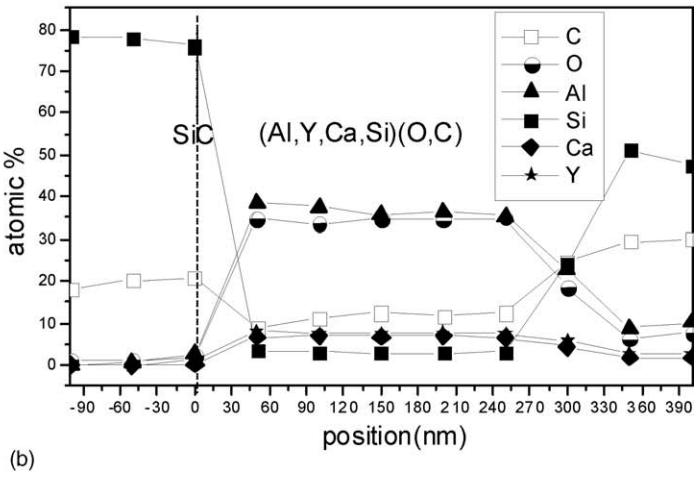

Fig. 5. (a) TEM micrograph of (Al,Y,Ca,Si)(O,C) liquid phase attached to the SiC and (b) EDS profile across liquid/SiC interface according to dotted line in (a).

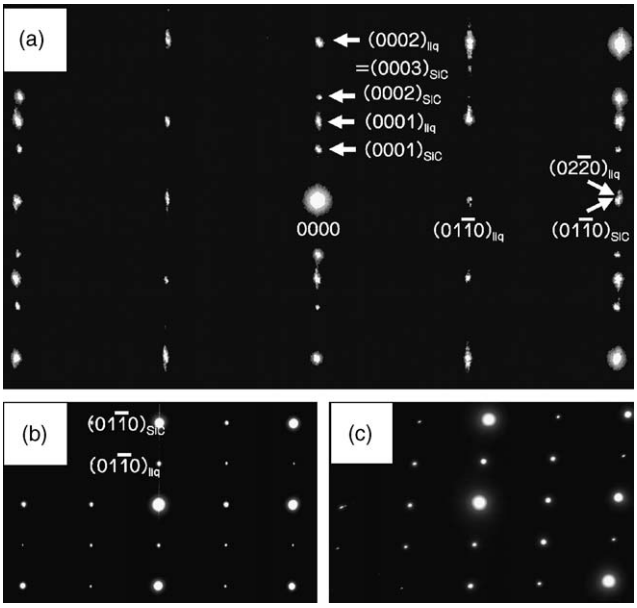

Fig. 6. Selected area diffraction pattern showing relationships between (Al,Y,Ca,Si)(O,C) liquid phase and 6H-SiC: (a) [2 1 $\bar{1}$ 0] zone axis (four times enlarged image), (b) [2 1 $\bar{1}$ $\bar{2}$] zone axis, and (c) [$\bar{8}$ 5 1 3 6] zone axis.

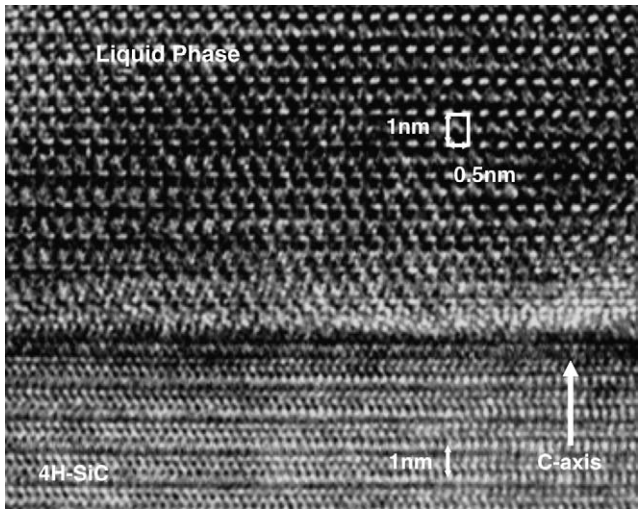

Fig. 7. High-resolution lattice image between crystallized liquid phase and SiC.

triple-junction phase was also composed of Al, Y, Ca, Si, O and C. Although its composition showed some fluctuation depending on the position, the average was estimated to be $(Al_1Y_{0.2}Ca_{0.19}Si_{0.08})(O_{0.95}C_{0.33})$ when normalized to Al. Note that the chemical composition of junction-phase is different from that of intergranular phase.

Fig. 6 shows typical selected area diffraction patterns (SADP) simultaneously taken from the junction phase and the α-6H SiC. The diffraction pattern and Kikuchi map analyses suggest that the crystallized junction phase has a hexagonal structure. The orientation relationship between the junction phase and the adjacent SiC grain is obvious in the overlapped diffraction pattern of Fig. 6(a), where the (0 0 0 3) reflection of 6H-SiC correspond to (0 0 0 2) reflection and (0 1 $\bar{1}$ 0) reflection to (0 2 $\bar{2}$ 0) of the junction phase. When 4H-SiC contacts with (Al,Y,Ca,Si)(O,C) phase, both of (0 0 0 1) reflections are identical, which means $\boldsymbol{c}_{SiC} = \boldsymbol{c}_{junction}$. Therefore, the axes in the two phases are parallel (***c***-axis//***c***-axis and ***a***-axis//***a***-axis) and lattice parameter relationships in ***a***-axis is $2\boldsymbol{a}_{SiC} = \boldsymbol{a}_{junction}$. The HREM image in Fig. 7 also shows the relationship between the triple-junction phase and SiC. However, the structure of junction phase is different from the crystallized intergranular films as already reported[13,22] in the as-sintered materials.

Zhan et al.[23] have examined the AYC-SiC specimen but they detected an amorphous intergranular film with a thickness of ∼1 nm with Y-ion segregation. In contrast, complete crystallization of both triple-junction phases and intergranular films has been observed in the present study. The differences between Zhan's experiment and the present can be pointed out as the followings: (1) the additive composition (7 wt.% Al_2O_3, 2 wt.% Y_2O_3, and 1 wt.% CaO for Zhan's sample whereas 5.7 wt.% Al_2O_3, 3.3 wt.% Y_2O_3, and 1 wt.% CaO for the present); they did not detect the presence of Ca at amorphous intergranular films, (2) the difference in polytype of starting SiC powders (97% β-SiC and 3% α-SiC for Zhan's sample whereas 100% α-SiC for the present); the difference in polytype of starting SiC powders may lead to the difference in β → α phase transformation during sintering,[5] (3) the difference in impurity contents (2 wt.% C and 1.24% oxygen for Zhan's β-SiC whereas 0.46% C and <0.85% oxygen for α-SiC in the present), and (4) the possible difference in cooling rate (Zhan et al. did not describe the cooling rate). Note, however, that the cooling rate (∼40 °C/min) of the present sintering process would not be faster than that adopted Zhan et al.[23]

On the other hand, from the SiC specimens prepared with Al_2O_3–Y_2O_3 additive with the same Al_2O_3:Y_2O_3 ratio used in this study, the presence of amorphous intergranular films with a thickness of ∼1 nm was detected.[24] Sigl and Kleebe[25] and Kim et al.[26] also fabricated SiC specimens with $Y_3Al_5O_{12}$ and they observed amorphous intergranular films and crystallized secondary phase in ternary junctions. In this regard, the complete crystallization of the boundary phase obtained in this study can be attributed mainly to the difference in the chemical composition of sintering additives. The chemical composition of the present additives (5.7 wt.% Al_2O_3, 3.3 wt.% Y_2O_3, and 1 wt.% CaO) might be a key factor for the crystallization of boundary phase during furnace cooling.

Comparing the results obtained previously[24] with those obtained in this study, the crystallization of boundary phase onto facets of SiC grains is expected to become easier by CaO. The effective catalysts which induce nucleation in glass forming medium are known[27] to exhibit a small lattice misfit (less than 10–15%) between nucleus and substrate. Furthermore, good molecular (or atomic) match between nucleus and substrate is important factor for an epitaxial nucleation.[28] It can

be postulated that the substitutional solid solution is formed when Ca is introduced into the junction phase. When Ca goes into a Y site, the lattice becomes expanded because the ionic radii of Ca^{2+} and Y^{3+} are 0.1000 and 0.0900 nm, respectively. This would decrease the lattice misfit between nucleus and substrate. We believe therefore that Ca (or CaO) has enhanced the crystallization of intergranular films. Note indeed that CaO is known[29] to be the effective nucleating agent in the glass-ceramics.

Previous results[30] on oxidation resistance of SiC ceramics showed that AYC-SiC have a better oxidation resistance than SiC with $Y_3Al_5O_{12}$ at 1400 °C, though the softening temperature in the Al_2O_3–Y_2O_3–CaO system is lower than that in Al_2O_3–Y_2O_3 system. The amorphous intergranular films in SiC with $Y_3Al_5O_{12}$ provide a rapid diffusion path for oxidation whereas crystalline nature of the intergranular films in AYC-SiC makes the ceramics oxidation-resistant.

4. Conclusions

1. Completely crystallized intergranular films, typically less than 1 nm in thickness, were observed in polycrystalline SiC without prolonged heat-treatment in the presence of Y_2O_3, Al_2O_3, and CaO as sintering additives. HREM image combined with EDS analyses confirmed that the crystallized films were hetero-epitaxially grown $(Al,Si)_2OC$ with 2H-type wurtzite structure. The Y and Ca segregations were also observed at grain boundaries.
2. Crystallized ternary junction phase had a topotactical relationship with SiC grains as $\boldsymbol{a}_{SiC}//\boldsymbol{a}_{junction}$, $\boldsymbol{c}_{SiC}//\boldsymbol{c}_{junction}$, and $\boldsymbol{a}_{SiC} = 2\boldsymbol{a}_{junction}$. The composition and structure of the ternary phase were different from those of intergranular films.
3. CaO addition is considered to be effective for the crystallization of intergranular film without prolonged heat-treatment.

Acknowledgments

The work at the University of Seoul was supported by Korea Research Foundation, under Grant no. KRF-2003-041-D00293. The authors are sincerely grateful to Prof. N.M. Hwang (Seoul National University) for stimulating discussion and Mr. S.H. Lee (University of Seoul) for help with plasma etching and SEM experiments.

References

1. Cutler, R. A., Virkar, A. V. and Hurford, A. C., *Liquid Phase Sintering of Silicon Carbide*. U.S. Patent 4,829,027, 9 May 1989.
2. Padture, N. P. and Lawn, B. R., Toughness properties of a silicon carbide with an in situ induced heterogeneous grain structure. *J. Am. Ceram. Soc.*, 1994, **77**, 2518–2522.
3. Winn, E. J. and Clegg, W. J., Role of the powder bed in the densification of silicon carbide sintered with yttria and alumina additives. *J. Am. Ceram. Soc.*, 1999, **82**, 3466–3470.
4. Padture, N. P., In situ-toughened silicon carbide. *J. Am. Ceram. Soc.*, 1994, **77**, 519–523.
5. Kim, Y.-W., Mitomo, M., Emoto, H. and Lee, J. G., Effect of initial α-phase content on microstructure and mechanical properties of sintered silicon carbide. *J. Am. Ceram. Soc.*, 1998, **81**, 3136–3140.
6. Cao, J. J., MoberlyChan, W. J., De Jonghe, L. C., Gilbert, C. J. and Ritchie, R. O., In situ toughened silicon carbide with Al–B–C additions. *J. Am. Ceram. Soc.*, 1996, **79**, 461–469.
7. Mitomo, M., Kim, Y.-W. and Hirotsuru, H., Fabrication of silicon carbide nano-ceramics. *J. Mater. Res.*, 1996, **11**, 1601–1604.
8. Kim, Y.-W., Mitomo, M. and Hirotsuru, H., Microstructural development of silicon carbide containing large seed grains. *J. Am. Ceram. Soc.*, 1997, **80**, 99–105.
9. Kim, J. Y., Kim, Y.-W., Mitomo, M., Zhan, G.-D. and Lee, J. G., Microstructure and mechanical properties of α-silicon carbide sintered with yttrium–aluminum garnet and silica. *J. Am. Ceram. Soc.*, 1999, **82**, 441–444.
10. Chen, D., Sixta, M. E., Zhang, X. F., De Jonghe, L. C. and Ritchie, R. O., Role of the grain-boundary phase on the elevated-temperature strength, toughness, fatigue and creep resistance of silicon carbide sintered with Al, B and C. *Acta Mater.*, 2000, **48**, 4599–4608.
11. Chen, D., Zhang, X. F. and Ritchie, R. O., Effect of grain-boundary structure on the strength, toughness, and cyclic-fatigue properties of a monolithic silicon carbide. *J. Am. Ceram. Soc.*, 2000, **83**, 2079–2081.
12. MoberlyChan, W. J. and De Jonghe, L. C., Controlling interface chemical and structure to process and toughen silicon carbide. *Acta Mater.*, 1998, **46**, 2471–2477.
13. Zhang, X. F., Sixta, M. E. and De Jonghe, L. C., Grain boundary evolution in hot-pressed ABC-SiC. *J. Am. Ceram. Soc.*, 2000, **83**, 2813–2820.
14. Jackson, T. B., Hurford, A. C., Bruner, S. L. and Cutler, R. A., SiC-based ceramics with improved strength. In *Silicon Carbide '87*, ed. J. D. Cawley and C. E. Semler. The American Ceramic Society, Westerville, OH, 1989, pp. 227–240.
15. Liden, E., Carlstrom, E., Eklund, L., Nyberg, B. and Carlsson, R., Homogeneous distribution of sintering additives in liquid-phase sintered silicon carbide. *J. Am. Ceram. Soc.*, 1995, **78**, 1761–1768.
16. Keppeler, M., Reichert, H. G., Broadley, J. M., Thurn, G., Wiedmann, I. and Aldinger, F., High temperature mechanical behavior of liquid phase sintered silicon carbide. *J. Eur. Ceram. Soc.*, 1998, **18**, 521–526.
17. Chen, D., Gilbert, C. J., Zhang, X. F. and Ritchie, R. O., High temperature cyclic fatigue-crack growth behavior in an in situ toughened silicon carbide. *Acta Mater.*, 2000, **48**, 659–674.
18. Sixta, M. E., Zhang, X. F. and De Jonghe, L. C., Flexural creep of an in situ-toughened silicon carbide. *J. Am. Ceram. Soc.*, 2001, **84**, 2002–2028.
19. Udalov, Y. P., Appen, Z. S. and Parshina, V. V., *Phase Diagrams for Ceramist* (*Vol VI, Fig. 6683*). The American Ceramic Society, 1987.
20. Hammel, J. J., Nucleation in glass-forming materials. In *Nucleation*, ed. A. C. Zettlemoyer. Marcel Dekker, New York, 1969, pp. 489–525.
21. Kingery, W. D., Bowen, H. K. and Uhlmann, D. R., *Introduction to Ceramics*. John Wiley & Sons, New York, 1991.
22. Bando, Y., Suematsu, H. and Mitomo, M., Grain boundary phase analysis of silcon nitride by a newly developed 300 kV field-emission electron microscope. *Mater. Res. Soc. Symp. Proc.*, 1994, **346**, 733–738.
23. Zhan, G. D., Ikuhara, Y., Mitomo, M., Xie, R. J., Sakuma, T. and Mukherjee, A. K., Microstructural analysis of liquid-phase-sintered β-silicon carbide. *J. Am. Ceram. Soc.*, 2002, **85**, 430–436.
24. Lee, S. H., Kim, Y.-W., Nishimura, T. and Mitomo, M., Role of the grain boundary phase on the high-temperature strength of silicon carbide sintered with Lu_2O_3 and AlN. *J. Am. Ceram. Soc.*, in preparation.
25. Sigl, L. S. and Kleebe, H. J., Core/rim structure of liquid-phase-sintered silicon carbide. *J. Am. Ceram. Soc.*, 1993, **76**, 773–776.

26. Kim, Y.-W., Mitomo, M. and Nishimura, T., Heat-resistant silicon carbide with aluminum nitride and erbium oxide. *J. Am. Ceram. Soc.*, 2001, **84**, 2060–2064.
27. Rabinovich, E. M., *Structure of Glass* (*Vol 3*), ed. E. A. Porai-Koshits. Consultants Bureau, New York, 1964, pp. 21–26.
28. Walton, A. G., Nucleation in liquids and solutions. In *Nucleation*, ed. A. C. Zettlemoyer. Marcel Dekker, New York, 1969, pp. 225–307.
29. Hedlund, A., *The Formation of Glass-Ceramics from OCF E-glass*. Final Report to the Center for Environmental and Energy Research at Alfred University, 31 September 2003.
30. Choi, H. J., Lee, J. G. and Kim, Y.-W., Oxidation behavior of liquid phase sintered silicon carbide with aluminum nitride and rare-earth oxides (Re_2O_3, where Re = Y, Er, Yb). *J. Am. Ceram. Soc.*, 2002, **85**, 2281–2286.